

Aberystwyth University

Snow cover and snow albedo changes in the central Andes of Chile and Argentina from daily MODIS observations (2000-2016)

Malmros, Jeppe K.; Mernild, Sebastian H.; Wilson, Ryan; Tagesson, Torbern; Fensholt, Rasmus

Published in:

Remote Sensing of Environment

DOI:

[10.1016/j.rse.2018.02.072](https://doi.org/10.1016/j.rse.2018.02.072)

Publication date:

2018

Citation for published version (APA):

Malmros, J. K., Mernild, S. H., Wilson, R., Tagesson, T., & Fensholt, R. (2018). Snow cover and snow albedo changes in the central Andes of Chile and Argentina from daily MODIS observations (2000-2016). *Remote Sensing of Environment*, 209, 240-252. <https://doi.org/10.1016/j.rse.2018.02.072>

General rights

Copyright and moral rights for the publications made accessible in the Aberystwyth Research Portal (the Institutional Repository) are retained by the authors and/or other copyright owners and it is a condition of accessing publications that users recognise and abide by the legal requirements associated with these rights.

- Users may download and print one copy of any publication from the Aberystwyth Research Portal for the purpose of private study or research.
- You may not further distribute the material or use it for any profit-making activity or commercial gain
- You may freely distribute the URL identifying the publication in the Aberystwyth Research Portal

Take down policy

If you believe that this document breaches copyright please contact us providing details, and we will remove access to the work immediately and investigate your claim.

tel: +44 1970 62 2400

email: is@aber.ac.uk

**Snow cover and snow albedo changes in the central Andes of Chile and Argentina
from daily MODIS observations (2000–2016)**

JEPPE K. MALMROS,¹, SEBASTIAN H. MERNILD,^{2,3,4}, RYAN WILSON,⁵,
TORBERN TAGESSON,¹, RASMUS FENSHOLT,¹

¹ *Department of Geosciences and Natural Resource Management, University of Copenhagen,
Copenhagen, DENMARK*

² *Nansen Environmental and Remote Sensing Center, Bergen, NORWAY,*

³ *Direction of Antarctic and Sub-Antarctic Programs, Universidad de Magallanes, Punta Arenas,
CHILE*

⁴ *Faculty of Engineering and Science, Western Norway University of Applied Sciences, Sogndal,
NORWAY*

⁵ *Department of Geography and Earth Sciences, Aberystwyth University, Aberystwyth, UK*

Resubmitted to Remote Sensing of Environment February 22nd, 2018

Corresponding author address:

Department of Geosciences and Natural Resource Management, University of Copenhagen, Øster
Voldgade 10, 1350 Copenhagen, Denmark.

E-mail: jkmalmros@gmail.com

Abstract

The variables of snow cover extent (SCE), snow cover duration (SCD), and snow albedo (SAL) are primary factors determining the surface energy balance and hydrological response of the cryosphere, influencing snow pack and glacier mass-balance, melt, and runoff conditions. This study examines spatiotemporal patterns and trends in SCE, SCD, and SAL (2000–2016; 16 years) for central Chilean and Argentinean Andes using the MODIS MOD10A1 C6 daily snow product. Observed changes in these variables are analyzed in relation to climatic variability by using ground truth observations (meteorological data from the El Yeso Embalse and Valle Nevado weather stations) and the Multivariate El Niño index (MEI) data. We identified significant downward trends in both SCE and SAL, especially during the onset and offset of snow seasons. SCE and SAL showed high inter-annual variability which correlate significantly with MEI applied with a one-month time-lag. SCE and SCD decreased by an average of $\sim 13 \pm 2 \%$ and 43 ± 20 days respectively, over the study period. Analysis of spatial pattern of SCE indicates a slightly greater reduction on the eastern side ($\sim 14 \pm 2 \%$) of the Andes Cordillera compared to the western side ($\sim 12 \pm 3 \%$). The downward SCE, SAL, and SCD trends identified in this study are likely to have adverse impacts on downstream water resource availability to agricultural and densely populated regions in central Chile and Argentina.

Keywords: Andes; Argentina; Chile; climate change; ENSO; MOD10A1; MODIS; snow albedo; snow cover extent; time series analysis.

63 **1. Introduction**

64 Snow in the semi-arid mountain regions of the central Andes of Chile and Argentina provides
65 important water resources to more than 10 million people and is of major importance for agriculture in
66 this area (Masiokas et al. 2006). Moreover, snow constitutes a key seasonal component in the surface
67 energy and hydrosphere budgets, reflecting incoming solar shortwave radiation (e.g., Konzelmann and
68 Ohmura 1995). Hydrological balance in the cryosphere is highly influenced by the amount of snow
69 precipitation and the spatiotemporal variability of seasonal snow cover extent (SCE). The combined
70 variability of snow precipitation, SCE, and snow cover duration (SCD) directly influences river-runoff
71 variabilities and glacier surface-mass balance conditions (Ragettli et al. 2016; Wilson et al. 2016).

72 On high mountain glaciers, energy availability for snow and ice melt is regulated by surface
73 albedo which is defined as the ratio of incoming solar radiation reflected by a surface (Cuffey and
74 Paterson 2010). Fresh snow, for example, acts as a near perfect reflector with albedo values of up to
75 0.98. However, snow albedo (SAL) diminishes over time as a result of snow metamorphism,
76 decreasing to as low as 0.46 (Cuffey and Paterson 2010). Rainfall can further enhance this natural
77 lowering of SAL through the addition of latent energy, which can initiate melting (Benn and Evans
78 2010) and cause downwasting and thinning of glaciers (Neckel et al. 2017). Snow and ice albedo can
79 also be reduced by the surface deposition of dust and/or anthropogenic soot (Hansen and Nazarenko
80 2004; Cereceda-Balic et al. 2012). In the central Andes, an additional factor which influences SAL is
81 the seasonal formation of penitents. Often forming in areas of low humidity and high solar elevation,
82 snow penitents can result in significant changes in the surface roughness of snow-covered terrain,
83 which, in turn, influences SAL and sublimation conditions (Corripio and Purves 2006).

84 The overall variability of SAL is influenced by a variety of factors: snow grain size, levels of
85 contamination, solar zenith angle, cloud cover, snow metamorphism, surface roughness, age factor, and
86 liquid water content, amongst others (Warren and Wiscombe 1980; Mernild et al. 2015a). Since SAL is
87 a key parameter determining the amount of energy available for surface melting snow and ice, snow-
88 sublimation, and metamorphosis, spatiotemporal variability in SAL is important when determining
89 snow ablation conditions (Male and Granger 1981; Brock et al. 2000; Hock 2005; Gardner and Sharp
90 2010; Mernild et al. 2016a).

91 Spatiotemporal trends in SCE and SAL interpolated from point measurements often include
92 large errors, especially in remote mountainous regions characterized by limited ground observations,

93 localized climate conditions and complex terrain. In comparison, satellite-based remote sensing and
94 satellite derived snow cover products provide opportune sources of large-scale SCE and SAL
95 measurements and have been successfully used as key inputs in climate, atmospheric and hydrological
96 models (Farr et al. 2007; Mernild et al. 2008; Vuille et al. 2008; Mernild et al. 2015a). Remote sensing
97 systems acquiring data from the visible (VIS) to shortwave infrared (SWIR) spectrum with a high
98 temporal resolution are well suited for monitoring SCE and SAL over large areas, providing good
99 spatial and temporal coverage (Wiscombe and Warren 1980; Dozier and Frew 1981; Dubayah 1992;
100 Knap et al. 1999).

101 Several remote sensing based snow cover products are currently available, most of which apply
102 either the normalized difference snow index (NDSI) (Hall et al. 1995), empirical relationship
103 assumptions or spectral un-mixing models (Klein and Stroeve 2002a). Optical sensor systems,
104 however, are unable to acquire useful information during cloudy conditions (Justice et al. 1998;
105 Marchane et al. 2015). Therefore, frequent satellite observation revisits are essential to study changes
106 in SCE and SAL, since surface conditions can vary rapidly and may change considerably over a few
107 days.

108 To compensate for extensive cloud cover, compromises are often made by conducting satellite
109 analysis based on composite products such as the MODIS (Moderate Resolution Imaging
110 Spectroradiometer) 8 day snow cover MOD10A2 product (Hall et al. 2002), which can mask subtle
111 changes in SCE and SAL over time. In order to avoid this limitation, the MODIS MOD10A1
112 Collection 6 (C6) dataset was used this study. MOD10A1 provides daily SCE and SAL values globally
113 at a spatial resolution of 500 m, making it suitable for evaluating seasonal trends in SCE and SAL (Hall
114 et al. 2002; Liang et al. 2005; Marchane et al. 2015; Hall and Riggs 2016; Saavedra et al. 2016; Li et al.
115 2017; Huang et al. 2017; Dariane et al. 2017), snow cover phenology (Xu et al. 2017) and the relation
116 between SCE and climate (Gurung et al. 2017; Li et al. 2017). Using MOD10A1 data, this study
117 analyses spatiotemporal changes in SCE and SAL in the central Andes of Chile and Argentina by
118 parameterizing a time series of seasonal SCE and SAL metrics at the per-pixel level. Furthermore, this
119 study examines the large-scale influence of ENSO events on SCE and SAL as well as the more
120 localized effect of climatic variability (utilizing meteorological data from the El Yeso Embalse (EYE)
121 and Valle Nevado (VN) automatic weather stations (AWS)) and elevation.

122

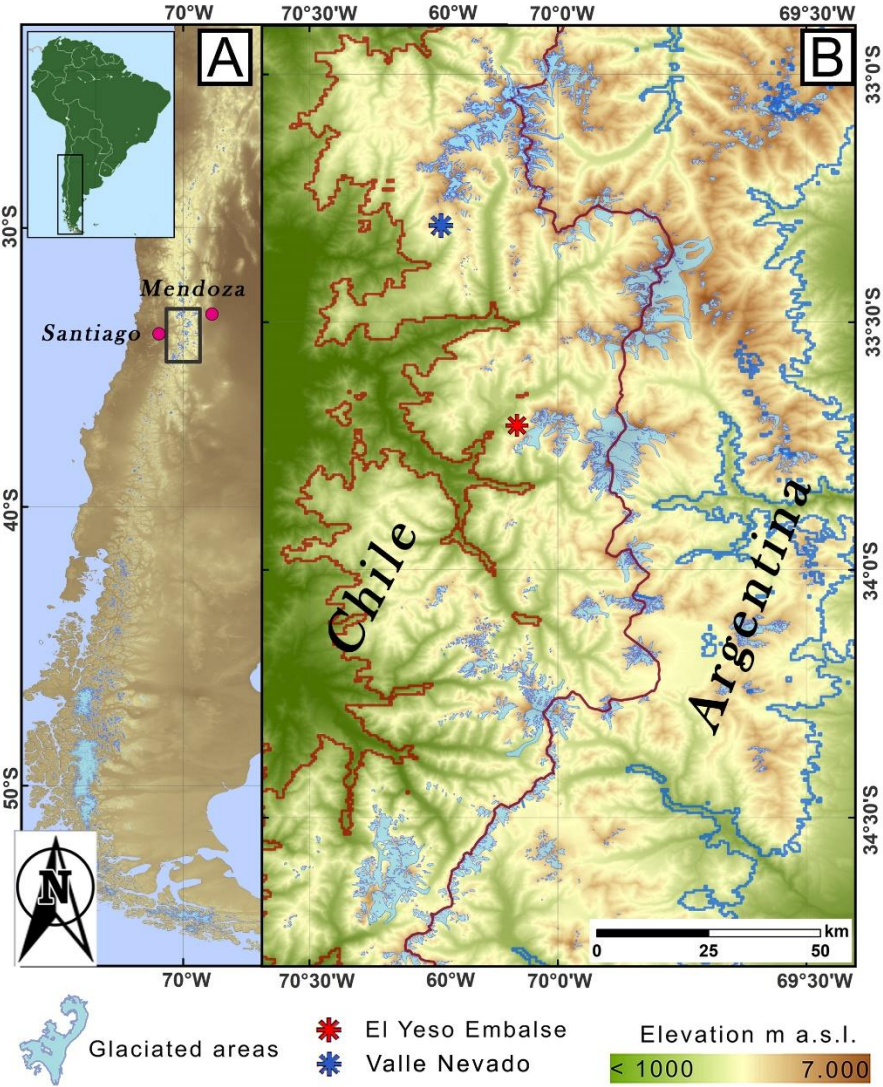
2. Study area

The Andes of central Chile and Argentina (31°S and 40°S) contain some of the highest peaks of the entire Andes Cordillera, reaching altitudes above 6,000 m above sea level (a.s.l.) (Fig. 1). Covering an area of ~1,730 km², the study area chosen is located immediately west of Santiago de Chile (32°50' – 34°50'S; 69°20' – 70°40'W). This study area includes several river basins which supply freshwater to large downstream populations (10+ million people in Chile and 2+ million in Argentina), hydro-power stations, and agricultural lands on both sides of the cordillera (Corripio and Purves 2006). This area of the central Andes also includes the largest glaciated areas in South America outside southern Patagonia (Saavedra et al. 2016). River runoff in this central region originates primarily from snowmelt (Masiokas et al. 2006), with snowfall contributing up to ~85 % of runoff from specific catchments (Mernild et al. 2016b). The availability of snow as a freshwater resource is therefore of vital socio-economic importance in this semi dry region (Peña and Nazarala 1987; Meza et al. 2012; Carey et al. 2017).

The intra-annual variability of precipitation in central Andes is highly influenced by the placement of an atmospheric high-pressure cell over the southeastern Pacific Ocean. This cell normally inhibits precipitation in the Austral summer (December – February) and allows for the passage of westerlies and frontal precipitation during Austral winters (June – August) (Garreaud et al. 2009). Precipitation events are usually concentrated between April and October, providing ~95 % of the mean annual totals, peaking in June or July (Masiokas et al. 2016). The strength of El Niño Southern Oscillation (ENSO) influences inter-annual variability in precipitation, with higher/lower precipitation occurring during El Niño/La Niña events (Rutllant and Fuenzalida 1991; Escobar et al. 1995; Leiva 1999; Montecinos and Aceituno 2003; Garreaud et al. 2009). During El Niño events, precipitation increases predominantly during the austral winter (Masiokas et al. 2006; McClung 2013). Whilst El Niño events do influence precipitation amounts, these events shows little or no significant signal in annual mass balance measurements of glaciers located in the central Andes but has been linked to the Pacific Decadal Oscillation (PDO) rather than the ENSO (Mernild et al. 2015a).

Along the central Andes, annual accumulation of snow is highest at 4,000 – 5,000 m a.s.l., where glacier accumulation zones are also present (Cornwell et al. 2016; Mernild et al. 2016b; Mernild et al. 2016c). Precipitation differences observed between the western and eastern sides of the Andes Cordillera occur due to the combination of orographic effects of the mountain relief and the dominating

153 westerly wind direction which results in precipitation amounts and humidity being lower on the eastern
 154 Cordillera slopes (Cornwell et al. 2016; Mernild et al. 2016b).
 155 For the central Andes, mean surface air temperatures are normally highest between December
 156 and March and lowest in July and August (Masiokas et al. 2016) and temperatures in the Andes showed
 157 increasing trends from 1975 to 2006 ($\square 0.25^{\circ}\text{C}/\text{decade}$) (Falvey and Garreaud 2009). The 0°C isotherm
 158 for the western side of the cordillera (40 km northeast of Santiago de Chile), was located at 3,385 m
 159 a.s.l. between 2009 and 2014 (Mernild et al. 2016c).
 160



161
 162 Figure 1: (a) The central Andes of Chile and Argentina; and (b) including the area of interest west and
 163 east snow cover regions delineated by red and blue lines, respectively. The divide between the western

164 and eastern Andes also represents the natural border (continental divide) between Chile and Argentina.
165 Blue areas represents glaciers. The red star in the center of the study area represents the location of the
166 El Yeso Embalse (EYE) meteorological station (2475 m a.s.l.) and the blue star the Valle Nevado (VN)
167 meteorological station (3050 m a.s.l.).

168

169 **3. Data**

170

171 *3.1 MODIS data*

172 The MOD10A1 C6 (henceforth MOD10A1 unless other version is implied) snow product is
173 derived from daily data acquisitions by the MODIS sensor aboard the Terra spacecraft (Riggs et al.
174 2017). The MODIS global daily snow cover product MOD10A1 (MODIS/Terra Snow Cover Daily L3
175 Global 500m Grid) is derived from cloud free observations and is well suited for regional snow cover
176 and albedo mapping (Hall et al. 2002; Liang et al. 2005; Dozier et al. 2008; Rittger et al. 2013; Fausto
177 et al. 2015; Mernild et al. 2015b). The latest MOD10A1 product was released in the spring of 2016 and
178 includes a range of improvements to the previous version including, amongst others, the removal of
179 Terra sensor degradation issues and improvements in atmospheric calibration (Lyapustin et al. 2014).
180 Importantly, the algorithms used to compile the MOD10A1 snow product are modified to include only
181 the best quality observations from the atmospherically corrected MOD10GA product (Hall et al. 2002).
182 Individual MOD10A1 product parts include NDSI, NDSI snow cover (SCE), SAL and corresponding
183 quality control flags. The MOD10A1 NDSI SCE is produced by using an empirical relationship with
184 NDSI values, where NDSI values are multiplied by a constant (Dozier et al. 2008; Hall and Riggs
185 2016). By using only full snow cover pixels, the accuracy of the MOD10A1 SAL product is improved
186 in terms of ground truth comparisons (Sorman et al. 2007; Mernild et al. 2015b). The overall error of
187 the MOD10A1 SAL product can vary substantially but is in the order of 1–10 % for good observations
188 with low atmospheric disturbances across the Greenland ice sheet (Klein and Stroeve 2002b). The
189 overall error at this location is likely higher due to the complex terrain of the Andes Mountains.
190 However, changes in albedo can still be quantified and here we opted for a per-pixel temporal change
191 analysis that is expected to mitigate the influence of topography to some degree by avoiding direct
192 inter-comparison of pixels influenced by different slope/aspect.

MOD10A1 data used in this study was obtained from the NASA Earth Observation System Data and Information System (EOSDIS) Reverb ECHO website (<https://reverb.echo.nasa.gov/>). Out of the 5,844 potential scenes available between March 1 2000 and Feb 29 2016, only 121 (~2 %) were missing in the archive, with a maximum temporal gap of 17 days. The snow cover year (season) was set to start 1 March and end February 28 (29) based on analysis of the data set. Pixels with cloud cover or poor retrievals were omitted as determined from QA flags and only pixels flagged as “best quality” were included in the further analysis (see section 4.1). Out of all pixels in the data series 74.8 % contained “best quality” data (supplementary material S1).

3.2 Ancillary data

Elevation data were obtained from the Shuttle Radar Topography Mission (SRTM) v.3. SRTM provides elevation data at a spatial resolution of 30 meters with an overall vertical accuracy of ~10 m and geo-position error of ~9 m (Farr et al. 2007). Multivariate El Niño index (MEI) ranks were obtained from the National Oceanic and Atmospheric Administration (NOAA) website (<http://www.esrl.noaa.gov/psd/enso/mei/table.html>). The MEI provides a ranked index of the strength of El Niño and La Nina events. MEI values are normalized for each bimonthly season (Wolter and Timlin 2011) and cover the 16-year study period of snow cover and snow albedo observations.

We acquired mean monthly air temperature (MMAT), mean annual air temperature (MAAT), and monthly precipitation sums (2000–2016) from the El Yeso Embalse meteorological station (EYE) supported by available data from the Valle Nevado (VN) meteorological station from 2013 onwards (locations in Fig. 1; data shown in supplementary material S2 and S3) from Dirección General de Aguas (DGA; www.dga.cl) and CryoNET respectively (<http://globalcryospherewatch.org/cryonet/sitepage.php?surveyid=68>). Finally, glacier outlines were obtained from the Randolph glacier inventory v. 5.0 (Pfeffer et al. 2014) in combination with updated glacier shapes from 2013/2014 (Malmros et al. 2016).

4. Methods

4.1 Time series preprocessing

The MOD10A1 time series was preprocessed and analyzed using the program TIMESAT (Jönsson and Eklundh 2002, 2004; Eklundh and Jönsson 2015). TIMESAT originally developed to analyze vegetation seasonality can be applied to all remote sensing data containing seasonal variability. We applied a Savitzky-Golay filter within TIMESAT to smooth the MOD10A1 time-series by applying polynomial fitting to the data points within a moving window of a certain width (Savitzky and Golay 1964; Jönsson and Eklundh 2004). Missing dates were filled with blank scenes before smoothing (Jönsson and Eklundh 2002) in order to compose a complete time series. Pixels not flagged as “best quality” from the MOD10A1 QA flags were excluded from the analysis. The width of the moving window influences the degree of smoothing and the ability of the filter to cope with rapid changes (parameters used in the TIMESAT preprocessing are shown in Table 1). The polynomial fitting was iterated and adapted to the upper part of the curve by assigning weights to data points above and below the result of the previous step (Jönsson and Eklundh 2004). SCD was extracted in TIMESAT for SCE, and the seasonal snow cover integral (SCI) (defined as the integral under the curve between onset and end of seasonal snow cover) was extracted to evaluate the accumulated seasonal SCE for each season. Areas characterized by limited seasonal variability were masked out due to the inability of the TIMESAT algorithm to estimate SCD for such conditions. The mask was created from the median of the 16 seasons and excluded areas with less than 16 days in the SCD dataset. Most excluded areas were located in glacier accumulation zones where constant snow cover prevents seasonal variability in SCE.

Table 1: Input parameters for use in TIMESAT.

Parameter	NDSI Snow Cover	Snow Albedo
Seasonal parameter	0.7	0.7
Number of envelope iterations	3	3
Adaptation strength	2	2
Savitzky-Golay window size	15	15
Spike Method	Median filter	Median filter
Amplitude season start (%)	70	65
Amplitude season end (%)	20	46

4.2 Trend estimation

We conducted linear temporal trend analysis to estimate the magnitude and direction of changes in SCE, SAL, SCD, SCI, MAAT, and annual precipitation. We calculated per-pixel trends by applying a nonparametric linear regression model with time as the independent variable and the abovementioned variables as dependent variables. Since time series of the variables analyzed often do not meet parametric assumptions of normality and homoscedasticity, a median trend (Theil–Sen, TS) procedure was applied using the Theil–Sen slope estimator (median trend) which has proven robust against outliers (Eastman 2009). Uncertainty estimates of trends are calculated from standard deviations of the calculated metrics and are provided as \pm values to all trends reported. The significance of the trends was determined using the nonparametric Mann–Kendall test of significance (Mann 1945; Kendall 1975). The Mann–Kendall significance test is commonly used as a trend test for the TS median slope operator (Eastman 2009) and produces outputs of z-scores that allow for the assessment of both the significance and direction of trends. The trends were considered significant at $p < 0.05$ (where p denotes the probability that there is no significant difference between observations over time). Trends in SCE, SCD, and SCI were extracted from the area of maximum values (minimum of 75% at any given time) for the entire study period and similar for SAL.

5. Results

5.1 Spatio-temporal patterns in snow cover extent

Statistical analysis of the MODIS time series revealed that the minimum, median, and maximum SCE for the entire observation period and area (Fig. 2) was 2 %, 43 %, and 74 %, respectively. SCE showed the presence of a clear linear relationship with elevation (coefficient of determination (r^2) = 0.95, $p < 0.01$; Fig. 2d). However, the relationship was imperfect ($r^2 = 0.34$) above 4,000 m a.s.l due to increased scattering in the accumulation zone of the glaciers. At its maximum, SCE covered 1,730 km² (74%) of the study area, only being present at elevations above 1,250 m a.s.l. SCE area was normally distributed with highest concentration of SCE observed between 3,250 and 4,000 m a.s.l. (Fig. 2e). SCE was on average ~11 % less on the eastern side of the Cordillera compared to the west (Fig. 2a-c).

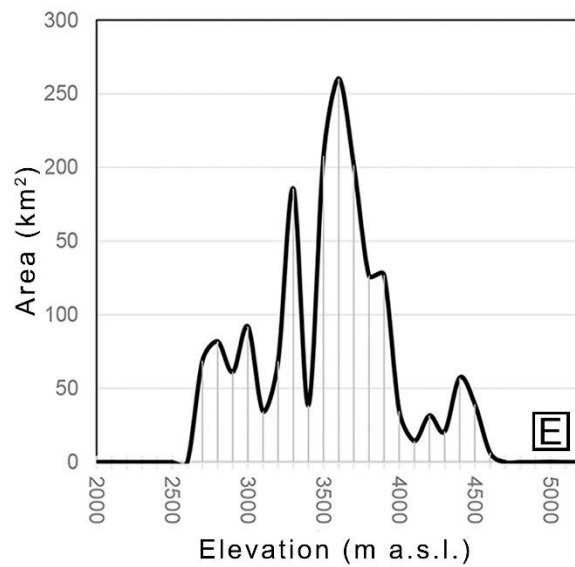
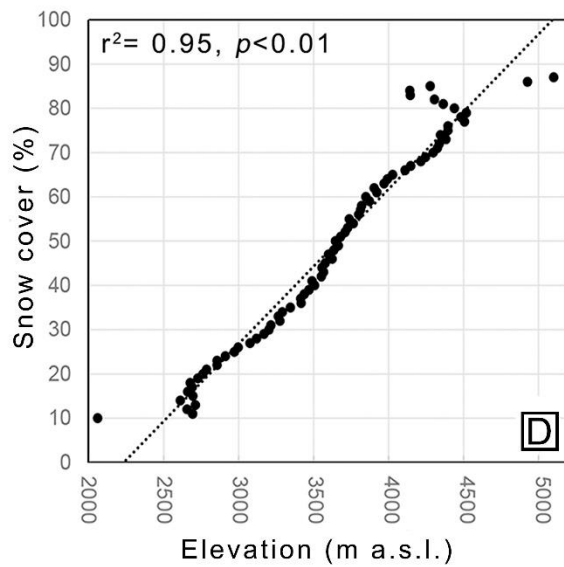
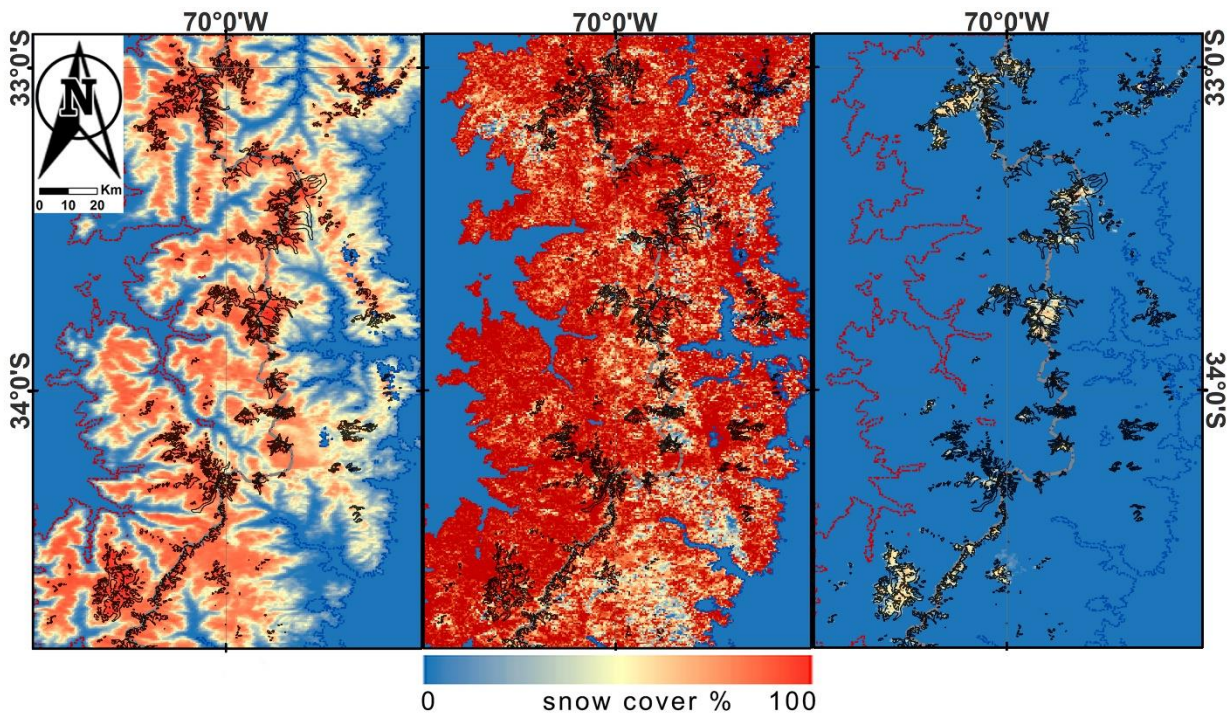
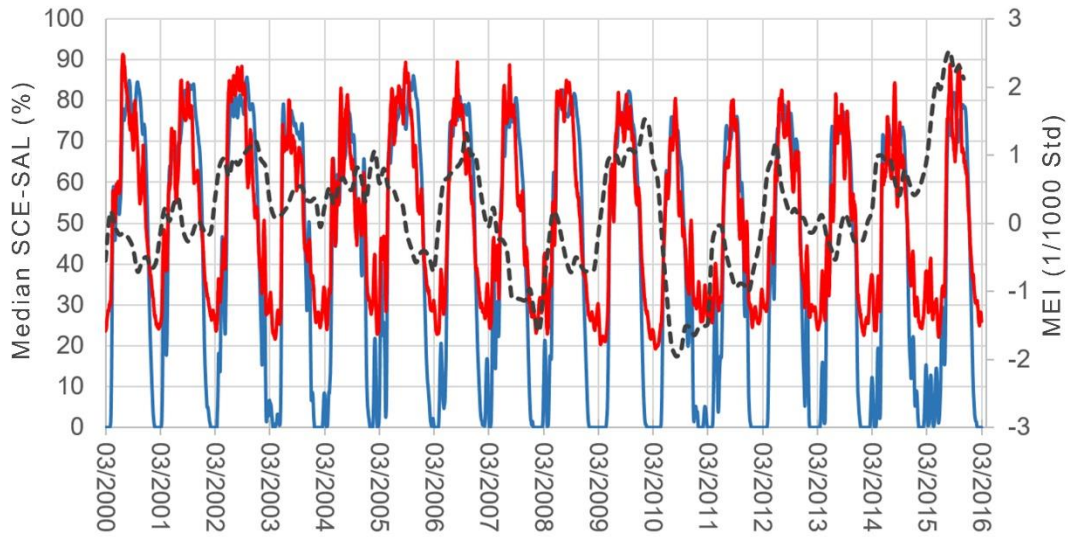


Figure 2: a) Median snow extent; b) maximum snow cover extent; c) minimum snow cover extent for the 16 snow seasons observed (2000–2016) (glaciers are delineated by black); d) Mean SCE change with elevation; and e) Snow covered area distribution with elevation.

5.2 Inter- and intra-annual variability in snow cover extent (SCE) and snow albedo (SAL)

280 The mean SCE over the study area between 2000 and 2016 was approximately ~25 % in austral
 281 summer and ~68 % in austral winter, reaching a maximum between July 24th and 25th October and a
 282 minimum in autumn between March 6th and June 6th (Fig. 3). Overall, spatial trends for SCE and SAL
 283 showed widespread downward tendencies (Fig. 4). For SCE, downward trends dominated, with
 284 medium SCE decreasing by 13.4 ± 4.0 % between 2000 and 2016 (0.35 % yr^{-1}). Demonstrating spatial
 285 variabilities, the downward trends in SCE were found to be more pronounced for the the eastern side of
 286 the Cordillera (13.9 ± 4.0 %, 0.9 % yr^{-1}) compared to the west (12.4 ± 3.1 %, 0.8 % yr^{-1}). The eastern side
 287 of the Cordillera also showed lower SCE but higher SCE variability compared to the western side, this
 288 despite the eastern side being more elevated (mean elevation for the western and eastern sides is 3,115
 289 m a.s.l and 3,720 m a.s.l, respectively) (Fig. 2d). Median SAL trends from March 2000 to February
 290 2016 were also downward with mean values decreasing by 7.4 ± 2.2 % (0.5 % yr^{-1}). Downward trends in
 291 SAL were shown to be more widespread in the southern parts of the study area compared to northern
 292 parts. However, we found no significant differences between the eastern and western sides of the
 293 Cordillera.



295
 296 Figure 3: Variation in daily median SCE (blue) and median SAL (red) percentage and the bi-monthly
 297 multivariate ENSO index (MEI) (dark dashed line) in 1/1000 standard variations (Wolter and Timlin
 298 2011).

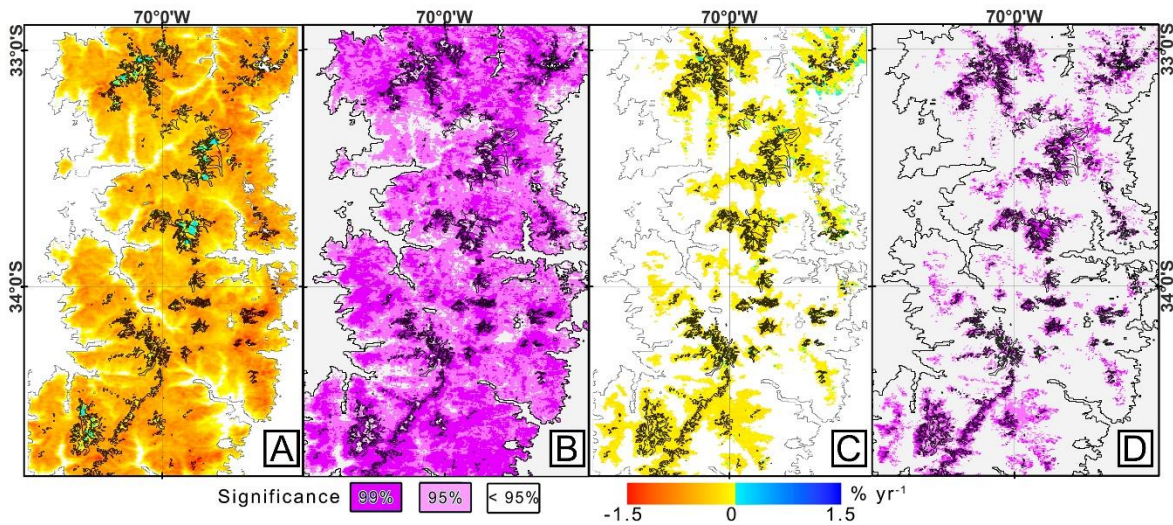


Figure 4: Linear median trend ($p < 0.05$) in: SCE (a) and SAL (c) from Mar 2000 through Feb 2016, and the corresponding significance level of each trend (b, d).

Comparisons with SRTM data, the SAL trends observed showed negative correlations below $\sim 4,600$ m a.s.l. ($-1.1 \pm 0.8 \text{ \% yr}^{-1}$, $r=0.84$, $p < 0.01$). Above $\sim 4,600$ m a.s.l., however, a distinct shift is observed, with increasing correlations as a function of elevation ($0.2 \pm 0.01 \text{ \% yr}^{-1}$, $r=0.83$, $p < 0.01$) (Fig. 5). In regards to intra-annual variability, SCE showed pronounced downward trends ($< -1 \text{ \% yr}^{-1}$) during the onset (April, May, and June) and offset (October, November, December, and January) of the snowy season. In comparison to SCE, SAL showed slightly less intra-annual variability with most downward trends occurring during the onset of the snowy season (Fig. 6).

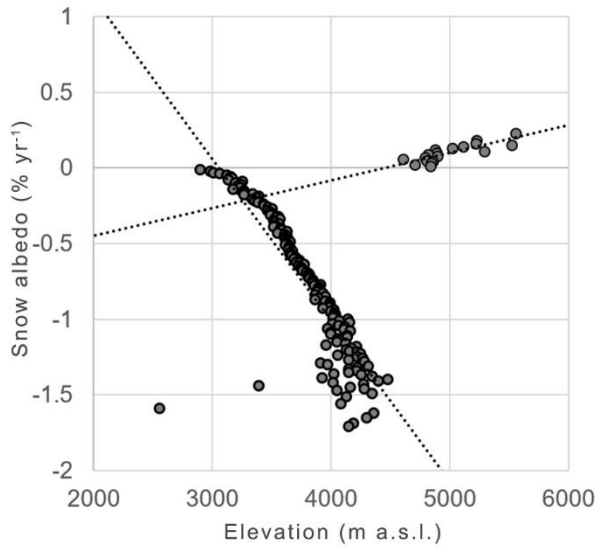


Figure 5: Trends in snow albedo (SAL) with elevation.

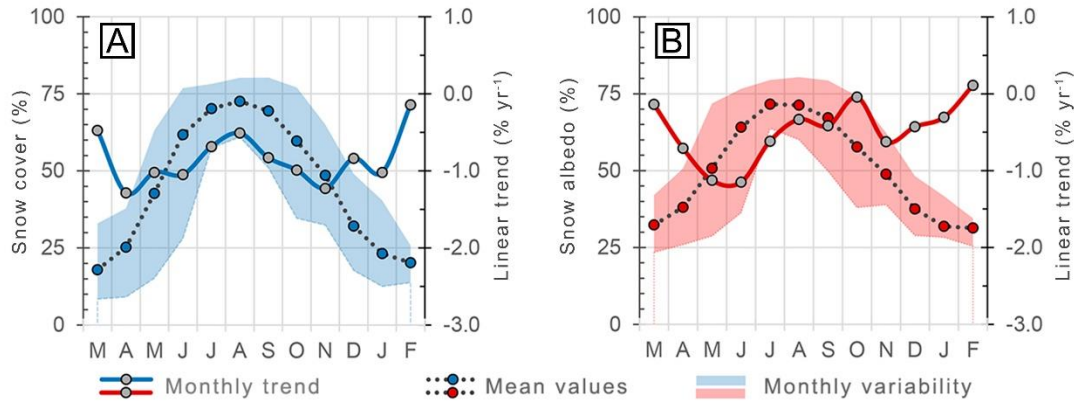
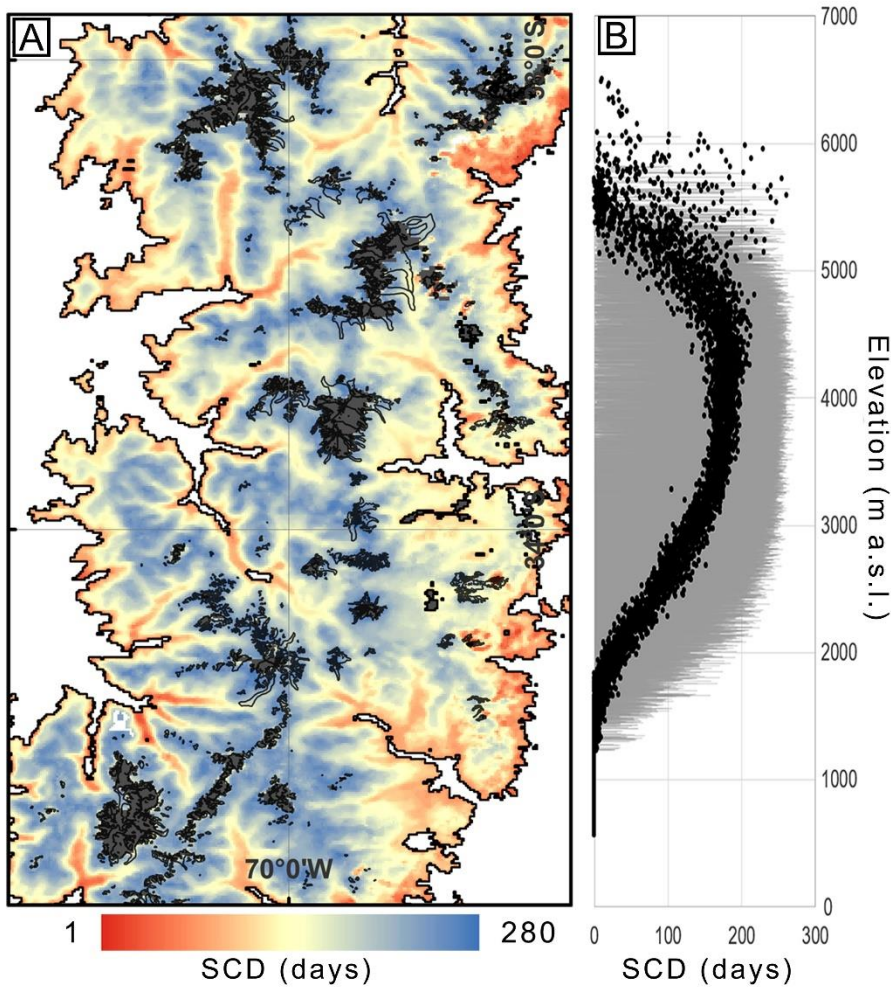


Figure 6: Intra-annual linear trends (blue and red lines), monthly mean values (dotted lines) and spread (colored areas; monthly minimum and maximum values) in: (a) snow cover extent (SCE); and (b) snow albedo (SAL) between 2000 and 2016.

5.3 Snow cover duration (SCD) and seasonal snow cover integral (SCI)

The seasonal SCD values ranged between 0 and 280 days and the seasonal mean SCD ranged between 203 days in the 2005–2006 to 130 days in 2011–2012, with an overall median of 173 days (Fig. 7a). We observed a strong correlation between SCD and elevation (excluding glacier areas). SCD, for example was shown to increase by an average of ~6 days for every 100-meter increment within the

326 2,000 to 4,600 m a.s.l. elevation range ($r^2=0.80$, $p<0.01$) (Fig. 7a). Overall, the trends in SCD were
 327 downward, showing a mean reduction of 43 ± 20 days for the study period (-2.7 ± 1.3 days yr^{-1}) (Fig.
 328 8a). Trends were especially negative on the eastern side of the Cordillera, with a reduction of 52 ± 36
 329 days (3.3 ± 2.3 days yr^{-1}), whereas on the western side SCD reduced by 35 ± 33 days (2.2 ± 2.0 days yr^{-1}).
 330
 331



332
 333 Figure 7: a) Median snow cover duration (SCD, days) 2000–2016 (dark grey areas represent locations
 334 where the model failed to determine seasonality); and (b) Mean snow cover duration with elevation for
 335 the 2000–2016 period (grey bars show the spread between minimum and maximum values of SCD as a
 336 function of elevation).
 337

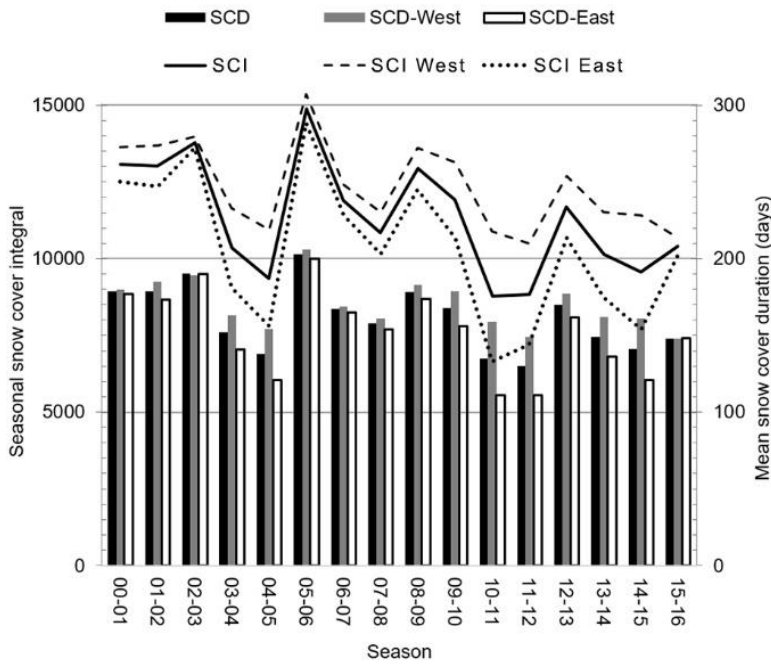
338

339 Figure 8: (a) Per pixel yearly snow cover duration (SCD) trend 2000–2016, and (b) corresponding
 340 significance of trend. Dark gray masked areas represent the mask where SCD values are erroneous and
 341 black lines represent glaciers.

342

343 The SCI for the entire study area declined by $1.5 \pm 0.5 \text{ \% yr}^{-1}$ (median trend), corresponding to 25 ± 8
 344 % during the full period of 16 snow seasons. The SCI also shows substantial inter-annual variation
 345 (Fig. 9), especially on the eastern side of the Cordillera, where SCI is on average 17 % smaller and
 346 trends are substantially more downward ($1.8 \pm 0.5 \text{ \% yr}^{-1}$) than for the western side ($1.2 \pm 0.4 \text{ \% yr}^{-1}$).

347



348

349 Figure 9: Mean snow cover duration (SCD, bars) and seasonal snow cover integral (SCI, lines) for the
 350 entire study area and for the western (SCD-W) and eastern (SCD-E) sides of the cordillera separately.

351

352 5.4 Impact of changes in temperature, precipitation, and El Niño Southern Oscillation (ENSO) on snow 353 cover duration and snow albedo

354

355 Analysis of the meteorological data available from the EYE AWS (Figure 1b) revealed a
 significant downward trend in precipitation of -4 mm yr^{-1} and an insignificant trend in MAAT of

356 0.05°C yr⁻¹ between 2000 and 2016. Between 2000 and 2009, nine extreme precipitation events (>200
357 mm month⁻¹) were identified, with the 2003-2004 season (March-February) receiving a maximum of
358 1,259 mm. These ‘extreme’ events occurred mostly during austral winters and account for large
359 differences in inter-annual precipitation amounts, SCE and SCD sums. Post 2009, no extreme
360 precipitation events occurred, however a minimum of 317 mm was observed for the 2014-2015 season.
361 The mean annual precipitation sum for the 2000 to 2016 observation period was 677 mm. MAAT for
362 this observation period was 9.0°C, with maximum and minimum values of 10.3°C and 7.3°C measured
363 for the 2003-2004 and 2011-2012 seasons, respectively.

364 Statistical comparisons between the MODIS-derived snow data and the observed EYE
365 meteorological data revealed that monthly SCE and SAL averaged over the study area and for the pixel
366 where EYE is located (in brackets) correlated strongly with MMAT (r^2 -values of 0.74 (0.71) and 0.82
367 (0.61), respectively) (Fig. 10a-b). For the VN met-station, the corresponding comparison between SCE
368 and MMAT also show a significant correlation for the 2013 to 2016 period (r^2 -values of 0.62). Mean
369 monthly SCE and SAL also correlate with monthly precipitation sums, but to a lesser extent (r^2 -values
370 of 0.20 (0.21) and 0.28 (0.19)) (Fig. 10c-d). In comparison, SCI correlated more strongly with annual
371 precipitation sums (r^2 -value of 0.84) (Fig. 10e).

372

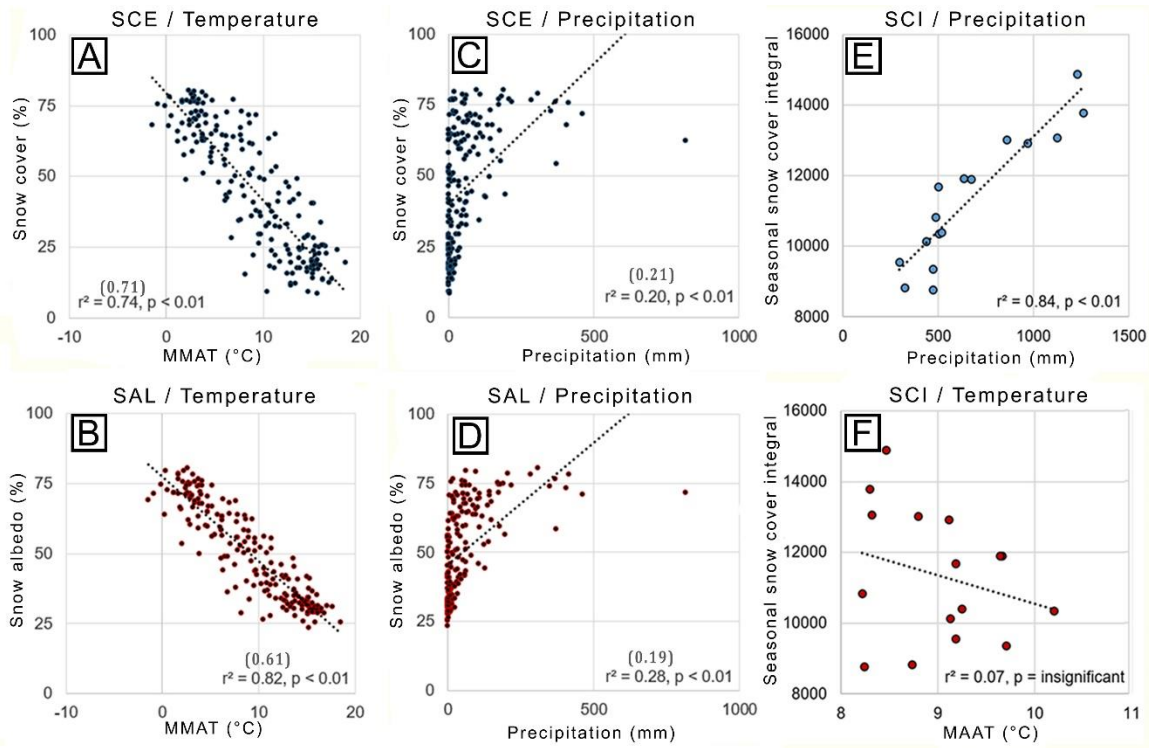
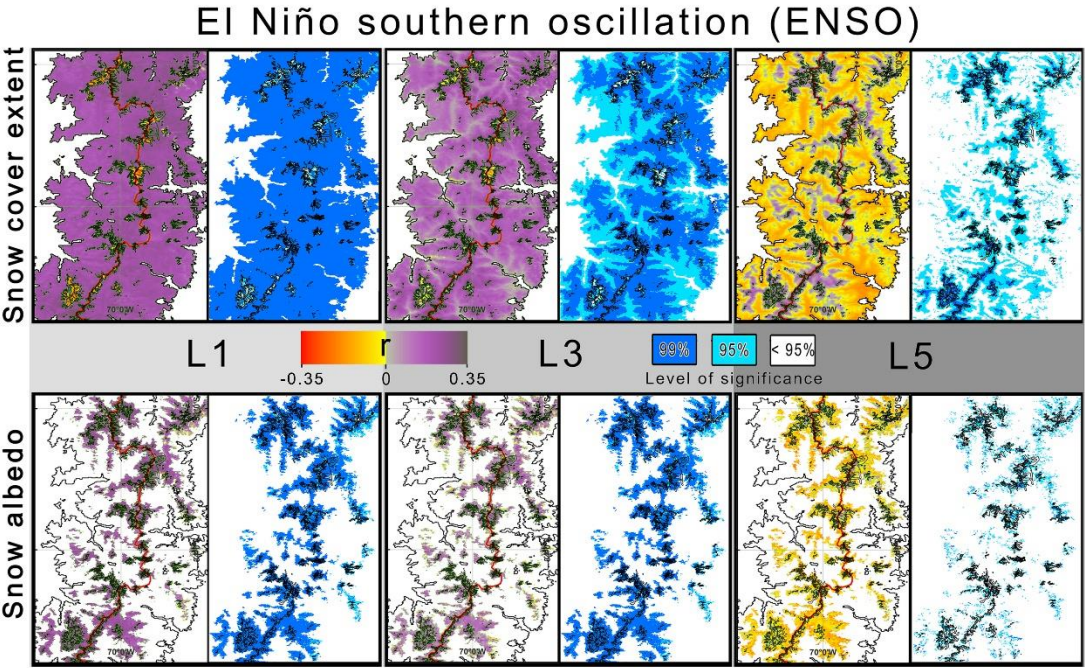


Figure 10: Relationships between monthly meteorological data (EYE station; Fig. 1) and monthly SCE, monthly SAL, and SCI averaged over the study area. a) Monthly SCE against MMAT; b) monthly SAL against MMAT, c) Monthly SCE against monthly precipitation sums, d) Monthly SCE against monthly precipitation sums, e) SCI against annual precipitation sums, and f) SCI against MAAT. r^2 -values between the EYE station data and the pixel where it is located is shown in brackets.

There can be large uncertainties introduced by comparing a single station with observations from a larger study area. However, currently it remains the only long-term continuous dataset available in the area, and trends from the local pixel and the station confirms the relationship with trends for the area in general (Fig. 10). Furthermore, EYE and NV temperature data significantly correlated (r^2 of 0.89) showing the temperature trends at EYE and NV being similar at least for that part of the western side of the cordillera in the 2013-2016 period.

ENSO events (MEI) (plotted in Fig. 3) show significant correlations with mean SCE and SAL values for the study area (Fig. 11). Mean correlation coefficient values (r) between MEI and SCE/SAL were strongest when a lag of one month (L1) was applied to the SCE/SAL time series (mean r -values

390 of 0.21 for the study area). Generally, glaciated areas where snow cover is already present are
 391 characterized by negative SCE and ENSO correlations for shorter lag periods (L1), which is in contrast
 392 to the surrounding snow covered areas. This pattern is reversed for longer lag periods (e.g., five
 393 months), when glaciated and higher elevated areas significantly correlate with ENSO, whereas
 394 surrounding lower altitude areas are characterized by negative correlations.
 395



396
 397 Figure 11: Per-pixel correlations and significance of SCE/SAL with the ENSO index (MEI) including
 398 one-, three- and five-month lag time (L1, L3, and L5). Red line demarks the east west divide.
 399

400 6. Discussion

402 6.1 Monitoring and assessment of snow cover and snow albedo

403 Spatio-temporal analysis of MODIS-derived SCE, SAL, SCD, and SCI data revealed significant
 404 changes during the observation period of this study. Key to the interpretation of these results is the
 405 quantification of sensor related errors and their influence on the trends observed (2000–2016).
 406 Unfortunately, only a few validation studies of the MOD10A1 C6 products have been published to
 407 date. Recent studies using MOD10A1 collection C6 for the Greenland ice sheet however found that

408 v.C6 corrects for the C5 temporal trend bias in dry snow areas and that albedo retrieval accuracy in C6
409 is substantially improved over C5 (Box et al. 2017; Casey et al. 2017). Therefore, the accuracy of this
410 product is expected to be better than or at least as good as the C5 product, which has been evaluated in
411 several previous studies (Tekeli et al. 2005; Hall and Riggs 2007; Gao et al. 2010; Arsenault et al.
412 2014; Marchane et al. 2015). These studies estimate an overall detection error ranging from ~5 % to
413 ~48 %, depending on locational properties and type of ‘ground truth’ observations used. In general,
414 spatially homogeneous locations with flat terrain produces less error than in complex terrain with
415 mixed surface as being the case for this study (Wang et al. 2014; Burakowski et al. 2015; Moustafa et
416 al. 2017). By applying a per-pixel temporal change analysis approach in the current study, thereby
417 avoiding direct inter-comparison of pixels characterized by different slope/aspect, the influence of
418 topography is expected to be reduced to some degree. This should also be seen in the context of the
419 latitudinal location of the study area (32°50’– 34°50’ S), characterized by an annual range in solar
420 zenith angles of 28-60 for MODIS overpass times. This makes the region less prone to influences from
421 mountain shadowing as compared to complex terrain of higher latitudes of the northern/southern
422 hemisphere. Snow detection in v.6 is expected to show improvements in comparison to previous
423 versions especially above 1.300 m a.s.l., where the surface temperature screen used in the product
424 algorithm (which has previously caused false negatives) has been rolled back leaving fewer gaps in the
425 data (Hall and Riggs 2016).

426 The smoothed and gap-filled MOD10A1 C6 dataset produced with TIMESAT is assumed to
427 correctly represent the seasonal snow distribution for the area. Here, only the best quality MOD10A1
428 C6 observations (by including information available from the QA flags; 0=“best quality”) were used
429 for the Savitzky-Golay function fitting in TIMESAT. By adjusting the data fitting to the upper
430 envelope of the daily observations, we ensured that the SCE and SAL values follow rapid changes,
431 which can occur in snow cover extent and albedo. The TIMESAT model uses local function fitting,
432 where values before and after in the time series are considered. This local function fitting reduces the
433 chance of error occurrence in the MOD10A1 observed snow cover (Tekeli et al. 2005). For the upper
434 ablation zones of glaciers, characterized by limited seasonal variability or year round snow SCE, it is
435 not possible to accurately assess seasonality variables and thereby SCD. In this case, a glacier mask
436 was applied based on SCE seasonal variability, in doing so, restricting the SCD analysis to non-

glaciated areas (Fig. 7a). Out of 709029144 individual pixel records in the time series 24.2 % were filled with modeled TIMESAT data.

Snow albedo detection in mountainous environments from remotely sensed imagery can contain large errors when measured on terrain with steep slopes. Validation of satellite or aerial imagery based data using stationary point albedometers can also be challenging because of pronounced mixed pixel and geolocation issues (Liang et al. 2005; Sorman et al. 2007; Mernild et al. 2015b; Box et al. 2017). However, these issues are not likely to have significantly influenced the trends observed in this study as the MOD10A1 pixels are measured in the same pixel location from year to year in a location where seasonal variation in solar zenith angle influence is relatively low (annual range between 28-60 degrees) compared to higher latitudes of the northern/southern hemisphere. MOD10A1 snow albedo is produced only for cloud free pixels with full snow cover (+50 %) indicating that for pixels characterized by limited full snow cover observations seasonal fitting could have influenced the accuracy of the TIMESAT generated data.

6.2 Analysis of climate variables

The analysis of the effect of local scale climatic variability presented in this study made use of two AWS's EYE and VN in the study area. Indeed, the use of a single or just two AWS's is not ideal when comparing measurements with the spatially large-scale MOD10A1 dataset. Furthermore, given the location of the AWS's on the western side of the cordillera and the presence of distinct climatic gradients (e.g. Mernild et al. 2016a), the data recorded is unlikely to be fully representative of the study area as a whole. However, this scarce coverage of ground observations reflects the general conditions for mountainous areas of the Andes and underlines the need for remotely sensed monitoring methods. Additionally, there is a need for high-resolution gridded meteorological products that work well in complex terrain. A high-resolution meteorological dynamical model combined with remote sensing derived products is likely to improve our understanding of the climatic variability impact on snow cover dynamics. Upward trends in MAAT have higher impact the lower the altitudes (mostly noticeable in the southern part of the study area) causing changes in onset and offset of snow seasons to be more sensitive to even small changes in temperature (Fig. 4). Low areas with small slope gradient show higher sensitivity to upward changes in MAAT in regards to snow accumulation. Especially the low elevated areas on the eastern side of the cordillera show the effect of increased MAAT.

Above 4,600 m a.s.l., SCD shows a considerable increase in variability (Fig. 7b). This however is not surprising as, in highly elevated zones where SCD can be dependent on localized terrain (slope and area of topographical shadow) and weather conditions. High wind speeds, for example, often make it less likely for snow cover to persist in certain areas despite high levels of solid precipitation.

6.3 Drivers of change on snow cover variables

Studies based on modeling, field measurements and remote sensing have provided insights into the past, current, and future impacts of climate change on snow conditions and runoff in the Andean river catchments of central Chile and Argentina (Pellicciotti et al. 2007; Apaloo et al. 2012; Delbart et al. 2015; Mernild et al. 2015a, 2016a, 2016c; Ragettli et al. 2016). A number of these studies have predicted that air temperatures in the central Andes will continue to increase. An increase in air temperature, together with seasonal changes in precipitation patterns, will likely result in a decrease in the amount of runoff from snow melt and an increase in the amount of runoff from rain (Cai et al. 2014; Mernild et al. 2016a, 2016c; Ragettli et al. 2016). Since the 1970's, precipitation events have generally become more intense but less frequent in central Chile (Falvey and Garreaud 2007; Garreaud et al. 2009). The EYE precipitation data, for example, shows a number of intense precipitation events (above 200 mm m⁻¹) during the 2000–2009 period. Interestingly, none of these 'intense' events occurred during the 2010–2016 period.

Per-pixel correlations between SCE/SAL and the Multivariate El Niño index (MEI) show that MEI has a strong and significant impact on inter-annual SCE/SAL variability in the region (Fig. 11). Although El Niño events are often associated with increases in precipitation, they can also be associated with increases in air temperature (Cai et al. 2014) which, together, can have a pronounced altitude dependent effect on snow cover during spring and autumn. An increase in air temperature, for example, causes the 0°C isotherm to ascend to higher elevations resulting in a larger proportion of precipitation falling as rain as opposed to snow. Mernild et al. (2016c) observed this phenomenon for the Olivares basin (33°12' S; 70°09' W) between 1979 and 2014, where precipitation has been increasingly falling as rain in recent years. This change in the partitioning of precipitation over mountainous areas can offset the positive effects of increased precipitation on snow accumulation, with rainfall often enhancing snow and ice melt rates on glacier surfaces. The significant spatial variation in

correlation between MEI and SCE for one-month lag, we suspect is caused by the presence of snow cover on glaciers giving negative or no correlation on short term but increasing correlations with time.

Reduction in SCE in this study has also been studied in modelling studies based on MERRA satellite data (Mernild et al. 2016b, 2016c) which estimate that snow cover extent in the central Andes has reduced $\sim 1.3\%$ per decade 2000–2014 (linear trend, for the b1 window in Fig. 1) (Mernild et al. 2016b). Mernild et al. (2016c) suggest that the largest decreases in snow cover have occurred within the 3,000–5,000 m a.s.l. elevation range, where more than 70 % of seasonal precipitation falls as snow. In comparison, the rate of SCE change observed in this study for the same period and area is significantly higher, with per decade reductions equating to $\sim 2.8\%$. This difference between the results presented here and in Mernild et al. (2016c) may either be an indicator of faster SCE reduction during the 2000–2016 period or highlight possible SCE overestimations in the MERRA model utilized by the latter. For other regions of the world snow cover reductions are well documented. In the Arctic, for example, a general decrease in the amount of snow has been observed between 1999 and 2009, together with reductions in maximum winter snow water equivalent, a later snow-cover onset in autumn and earlier snow-free date in spring, and a decreasing snow-cover duration (Liston and Hiemstra 2011). Indeed a warming trend especially during autumn has been identified at EYE (Burger et al. 2018) and correspond well with the later onset of snow seasons seen in the area (Fig. 6.). To sustain all year runoff, rivers of the central Andes rely on substantial contributions from snow and ice-melt, and river discharge here is strongly linked to snow cover changes (Delbart et al. 2015). Decreases in SCE at the magnitudes shown in this study has the potential to cause a substantial redistribution in seasonal runoff for this region, where $\sim 21\%$ of river runoff originates from snow- and ice- melt (increasing to $\sim 85\%$ during dry summers) (Peña and Nazarala 1987; Mernild et al. 2016a). Glaciers in the central Andes are shrinking and down wasting as a consequence of climate warming and changes in precipitation patterns (Masiokas et al. 2006; Bodin et al. 2010; Gacitua et al. 2015; Malmros et al. 2016). Although initially increasing, ice melt runoff will begin to reduce in the future as lowest elevation land ice disappears. If these ice/snow cover trends continue, runoff conditions will likely change, especially during spring, dry summers and periods of drought, affecting the future sustainability of freshwater resources in areas downstream of the central Andes (Peña and Nazarala 1987; Delbart et al. 2015; Saavedra et al. 2016; Carey et al. 2017; López-Moreno et al. 2017). Whether

this change in runoff will cause the low lying areas in the catchment to become wetter or drier is largely determined by local topography (Polk et al. 2017, López-Moreno et al. 2017).

Directly influencing the surface energy balance, the downward trends in SAL revealed in this study (Fig. 4) may possibly result in positive feedbacks in regards to snow and ice melt. This trend of darkening surfaces, either from reduced snow cover or from enhanced melt conditions, is likely to be reinforced by increasing air temperatures and decreasing precipitation (e.g., Mernild et al. 2016c). Another positive feedback could be initiated by the accumulation of dust and debris on glacier surfaces leading to more energy being absorbed and further melt conditions, especially on lower parts of glaciers (Hansen and Nazarenko 2004; Oerlemans et al. 2009; Arenson et al. 2015). Minimum glacier-wide albedo has shown to be a good predictor for glacier mass balances conditions for temperate glaciers (López-Moreno et al. 2017; Polk et al. 2017), which suggests that glaciers in the study area may have positive mass balances, at least for some of the years analyzed. Decreases in surface albedo have also been observed for many other glaciated parts of the world (Box et al. 2012; Tedesco et al. 2013; Abermann et al. 2014; Fausto et al. 2015; Mernild et al. 2015b). The mean albedo for the Greenland ice sheet ablation area (June–August), for example, declined by 22.9 % from 2000 to 2016 while dry snow areas only decreased by 1.2 % (Box et al. 2017). Increasing albedo values seen above 4.600 m a.s.l. (Fig. 5.) are likely contributed to by the increase in precipitation and the presence of dry snow conditions at high altitudes (Box et al. 2017).

The central Andes are dominated by two distinctly different climate systems. On the western side of the Cordillera the climate is influenced by oceanic atmospheric interactions, whereas on the eastern side the climate can be considered continental in type (Prohaska 1976). This difference in climate is highlighted in this study by the relatively weak correlation between SCE/SAL and MEI on the eastern side of the Cordillera compared to the west. A higher inter-annual variability in SCE and SCI and more downward trend on the eastern part may be contributed to continental climate conditions (Fig. 9) as also observed in Saavedra et al. 2017.

7. Conclusions and outlook

Overall, snow cover extent (SCE) and snow albedo (SAL) decreased by 13.4 ± 4 % and 7.4 ± 2 %, respectively, between 2000 and 2016. SCE showed more downward trends on the eastern side of the Andes Cordillera (13.9 ± 4 %), while SAL showed a uniform decline throughout the area. A seasonal

analysis revealed downward trends in SCE and SAL for all months of the year, with the largest decreases occurring during the onset (for SCE and SAL) and at the end of the snow seasons (for SCE) ($> 1\% \text{ yr}^{-1}$). SCE showed a near linear increase with elevation ($r^2=0.96$, $p < 0.01$), and largest relative losses occurring at elevations above 4.600 m a.s.l. outside glaciated areas. Spatial analysis of the SAL data revealed increasingly downward trends up to ~4,600 m a.s.l. in elevation. Above ~4,600 m a.s.l. this trend is reversed, likely because of permanent or semi-permanent dry snow conditions present in glacier accumulation zone. Snow cover duration (SCD) decreased on average by 43 ± 20 days throughout the study area between 2000 and 2016 with largest changes occurring at elevations below 4.500 m a.s.l. on the eastern side and 3.500 m a.s.l. on the western side.

TIMESAT was unable to extract SCD for glacier areas that were covered with snow for most of the year due to the lack of seasonal variation. Additionally, in situations of large variations in snow conditions occurring over a very short time period the Savitzky-Golay seasonal fitting process applied may introduce some errors. SCD trends for the study area indicate a shortening of the snow season between 2000 and 2016. SCI trends for the included glacial areas were also shown to be downward during this 16-year observation period (these being more pronounced on the eastern side of the Cordillera).

The impact of ENSO events, which influence largescale precipitation and temperature patterns in the study area, on the SCE, SCD, and SAL was shown to be evident. Per-pixel analyses revealed that ENSO positively influences SCE/SAL values most strongly with a one-month time-lag. Data available from the EYE meteorological station, between 2000 and 2016, reveals that the monthly SCE and SAL values are primarily determined by variations in temperature, whilst montly SCI values are determined mostly by precipitation. If the observed decline in SCE persist in the coming years, it will likely result in a seasonal redistribution of available downstream freshwater which may cause future problems for people and agriculture in the region.

Acknowledgements

We extend a special thanks to the editor and the reviewers for their insightful critique of this article. This work was supported by the Chilean Fondecyt Regular Competition under grant agreement #1140172. All data requests should be addressed to the first author. The authors have no conflict of interest.

References:

- Abermann, J., Kinnard, C., & MacDonell, S. (2014). Albedo variations and the impact of clouds on glaciers in the Chilean semi-arid Andes. *Journal of Glaciology*, 60, 183-191
- Apaloo, J., Brenning, A., & Bodin, X. (2012). Interactions between Seasonal Snow Cover, Ground Surface Temperature and Topography (Andes of Santiago, Chile, 33.5°S). *Permafrost and Periglacial Processes*, 23, 277-291
- Arenson, L.U., Jakob, M., & Wainstein, P. (2015). Effects of Dust Deposition on Glacier Ablation and Runoff at the Pascua-Lama Mining Project, Chile and Argentina. In G. Lollino, A. Manconi, J. Clague, W. Shan, & M. Chiarle (Eds.), *Engineering Geology for Society and Territory - Volume 1: Climate Change and Engineering Geology* (pp. 27-32). Cham: Springer International Publishing
- Arsenault, K.R., Houser, P.R., & De Lannoy, G.J.M. (2014). Evaluation of the MODIS snow cover fraction product. *Hydrological Processes*, 28, 980-998
- Benn, D.I., & Evans, D.J.A. (2010). *Glaciers and glaciation*. London: Hodder Education
- Bodin, X., Rojas, F., & Brenning, A. (2010). Status and evolution of the cryosphere in the Andes of Santiago (Chile, 33.5 degrees S.). *Geomorphology*, 118, 453-464
- Box, J.E., Fettweis, X., Stroeve, J.C., Tedesco, M., Hall, D.K., & Steffen, K. (2012). Greenland ice sheet albedo feedback: thermodynamics and atmospheric drivers. *The Cryosphere*, 6, 821-839
- Box, J.E., Van As, D., Steffen, K., Fausto, R.S., Ahlstrøm, A.P., Citterio, M., & Andersen, S.B. (2017). Greenland, Canadian and Icelandic land-ice albedo grids (2000–2016). *Geol. Surv. Den. Greenl. Bull.*, 38, 53-56
- Brock, B.W., Willis, I.C., & Sharp, M.J. (2000). Measurement and parameterization of albedo variations at Haut Glacier d'Arolla, Switzerland. *Journal of Glaciology*, 46, 675-688
- Burakowski, E.A., Ollinger, S.V., Lepine, L., Schaaf, C.B., Wang, Z., Dibb, J.E., Hollinger, D.Y., Kim, J., Erb, A., & Martin, M. (2015). Spatial scaling of reflectance and surface albedo over a mixed-use, temperate forest landscape during snow-covered periods. *Remote Sensing of Environment*, 158, 465-477

614 Burger, F., Brock, B., & Montecinos, A. (2018). Seasonal and elevational contrasts in temperature
 615 trends in Central Chile between 1979 and 2015. *Global and Planetary Change (In Press)*
 616 Cai, W., Borlace, S., Lengaigne, M., van Rensch, P., Collins, M., Vecchi, G., Timmermann, A.,
 617 Santoso, A., McPhaden, M.J., Wu, L., England, M.H., Wang, G., Guilyardi, E., & Jin, F.-F.
 618 (2014). Increasing frequency of extreme El Nino events due to greenhouse warming. *Nature*
 619 *Clim. Change*, 4, 111-116
 620 Carey, M., Molden, O.C., Rasmussen, M.B., Jackson, M., Nolin, A.W., & Mark, B.G. (2017). Impacts
 621 of Glacier Recession and Declining Meltwater on Mountain Societies. *Annals of the American*
 622 *Association of Geographers*, 107, 350-359
 623 Casey, K.A., Polashenski, C.M., Chen, J., & Tedesco, M. (2017). Impact of MODIS sensor calibration
 624 updates on Greenland Ice Sheet surface reflectance and albedo trends. *The Cryosphere*, 11,
 625 1781-1795
 626 Cereceda-Balic, F., Palomo-Marín, M.R., Bernalte, E., Vidal, V., Christie, J., Fadic,
 627 X., Guevara, J.L., Miro, C., & Pinilla Gil, E. (2012). Impact of Santiago de Chile urban
 628 atmospheric pollution on anthropogenic trace elements enrichment in snow precipitation at
 629 Cerro Colorado, Central Andes. *Atmospheric Environment*, 47, 51-57
 630 Cornwell, E., Molotch, N.P., & McPhee, J. (2016). Spatio-temporal variability of snow water
 631 equivalent in the extra-tropical Andes Cordillera from distributed energy balance modeling and
 632 remotely sensed snow cover. *Hydrology and Earth System Sciences*, 20, 411-430
 633 Corripio, J.G., & Purves, R.S. (2006). Surface Energy Balance of High Altitude Glaciers in the Central
 634 Andes: The Effect of Snow Penitentes. *Climate and Hydrology in Mountain Areas* (pp. 15-27):
 635 John Wiley & Sons, Ltd
 636 Cuffey, K.M., & Paterson, W.S.B. (2010). *The Physics of Glaciers*. Elsevier Science
 637 Dariane, A.B., Khoramian, A. & Santi, E. (2017). Investigating spatiotemporal snow cover variability
 638 via cloud-free MODIS snow cover product in Central Alborz Region. *Remote Sensing of*
 639 *Environment*, 202, 152-165.
 640 Delbart, N., Dunesme, S., Lavie, E., Madelin, M., & Goma, R. (2015). Remote sensing of Andean
 641 mountain snow cover to forecast water discharge of Cuyo rivers. *Journal of Alpine Research*,
 642 15
 643 Dozier, J., & Frew, J. (1981). Atmospheric Corrections to Satellite Radiometric Data over Rugged
 644 Terrain. *Remote Sensing of Environment*, 11, 191-205

644 Dozier, J., Painter, T.H., Rittger, K., & Frew, J.E. (2008). Time-space continuity of daily maps of
 645 fractional snow cover and albedo from MODIS. *Advances in Water Resources*, 31, 1515-1526
 646 Dubayah, R. (1992). Estimating Net Solar-Radiation Using Landsat Thematic Mapper and Digital
 647 Elevation Data. *Water Resources Research*, 28, 2469-2484
 648 Dumont, M., Gardelle, J., Sirguey, P., Guillot, A., Six, D., Rabatel, A., & Arnaud, Y. (2012). Linking
 649 glacier annual mass balance and glacier albedo retrieved from MODIS data. *The Cryosphere*, 6,
 650 1527-1539
 651 Eastman, J.R. (2009). IDRISI Taiga guide to GIS and image processing. *Clark Labs Clark University*,
 652 Worcester, MA
 653 Eklundh, L., & Jönsson, P. (2015). TIMESAT: A Software Package for Time-Series Processing and
 654 Assessment of Vegetation Dynamics. In C. Kuenzer, S. Dech, & W. Wagner (Eds.), *Remote*
 655 *Sensing Time Series: Revealing Land Surface Dynamics* (pp. 141-158). Cham: Springer
 656 International Publishing
 657 Escobar, F., Casassa, G., & Pozo, V. (1995). Variaciones de un glaciar de Montaña en los Andes de
 658 Chile Central en las últimas dos décadas. *Bulletin de l'Institut français d'études andines*, 24,
 659 683-995
 660 Falvey, M., & Garreaud, R. (2007). Wintertime Precipitation Episodes in Central Chile: Associated
 661 Meteorological Conditions and Orographic Influences. *Journal of Hydrometeorology*, 8, 171-
 662 193
 663 Falvey, M., & Garreaud, R.D. (2009). Regional cooling in a warming world: Recent temperature trends
 664 in the southeast Pacific and along the west coast of subtropical South America (1979-2006).
 665 *Journal of Geophysical Research-Atmospheres*, 114
 666 Farr, T.G., Rosen, P.A., Caro, E., Crippen, R., Duren, R., Hensley, S., Kobrick, M., Paller, M.,
 667 Rodriguez, E., Roth, L., Seal, D., Shaffer, S., Shimada, J., Umland, J., Werner, M., Oskin, M.,
 668 Burbank, D., & Alsdorf, D. (2007). The Shuttle Radar Topography Mission. *Reviews of*
 669 *Geophysics*, 45, n/a-n/a
 670 Fausto, R.S., van As, D., Antoft, J.A., Box, J.E., Colgan, W., & Team, P.P. (2015). Greenland ice sheet
 671 melt area from MODIS (2000-2014). *Geological Survey of Denmark and Greenland Bulletin*,
 672 57-60

673 Gacitua, G., Uribe, J.A., R., W., Loriaux, T., Hernandez, J., & Rivera, A. (2015). 50MHz helicopter-
674 borne radar data for determination of glacier thermal regime in the central Chilean Andes.
675 *Annals of Glaciology*, 56

676 Gao, Y., Xie, H.J., Yao, T.D., & Xue, C.S. (2010). Integrated assessment on multi-temporal and multi-
677 sensor combinations for reducing cloud obscuration of MODIS snow cover products of the
678 Pacific Northwest USA. *Remote Sensing of Environment*, 114, 1662-1675

679 Gardner, A.S., & Sharp, M.J. (2010). A review of snow and ice albedo and the development of a new
680 physically based broadband albedo parameterization. *Journal of Geophysical Research-Earth*
681 *Surface*, 115

682 Garreaud, R.D., Vuille, M., Compagnucci, R., & Marengo, J. (2009). Present-day South American
683 climate. *Palaeogeography Palaeoclimatology Palaeoecology*, 281, 180-195

684 Gurung, D. R., Maharjan, S. B., Shrestha, A. B., Shrestha, M. S., Bajracharya, S. R. and Murthy, M. S.
685 R. (2017). Climate and topographic controls on snow cover dynamics in the Hindu Kush
686 Himalaya. *Int. J. Climatol.*, 37: 3873–3882.

687 Hall, D.H., & Riggs, G. (2016). MODIS/Terra Snow Cover Daily L3 Global 500m Grid, Version 6. In
688 National Snow and Ice Data Center (NSIDC) (Ed.). Boulder, Colorado USA: NASA

689 Hall, D.K., & Riggs, G.A. (2007). Accuracy assessment of the MODIS snow products. *Hydrological*
690 *Processes*, 21, 1534-1547

691 Hall, D.K., Riggs, G.A., & Salomonson, V.V. (1995). Development of methods for mapping global
692 snow cover using moderate resolution imaging spectroradiometer data. *Remote Sensing of*
693 *Environment*, 54, 127-140

694 Hall, D.K., Riggs, G.A., Salomonson, V.V., DiGirolamo, N.E., & Bayr, K.J. (2002). MODIS snow-
695 cover products. *Remote Sensing of Environment*, 83, 181-194

696 Hansen, J., & Nazarenko, L. (2004). Soot climate forcing via snow and ice albedos. *Proceedings of the*
697 *National Academy of Sciences of the United States of America*, 101, 423-428

698 Hock, R. (2005). Glacier melt: a review of processes and their modelling. *Progress in Physical*
699 *Geography*, 29, 362-391

700 Huang, X., Deng, J., Wang, W., Feng, Q. & Liang, T. (2017). Impact of climate and elevation on snow
701 cover using integrated remote sensing snow products in Tibetan Plateau. *Remote Sensing of*
702 *Environment*, 190, 274-288.

703 Jönsson, P., & Eklundh, L. (2002). Seasonality extraction by function fitting to time-series of satellite
704 sensor data. *Ieee Transactions on Geoscience and Remote Sensing*, 40, 1824-1832

705 Jönsson, P., & Eklundh, L. (2004). TIMESAT - a program for analyzing time-series of satellite sensor
706 data. *Computers & Geosciences*, 30, 833-845

707 Justice, C.O., Vermote, E., Townshend, J.R.G., Defries, R., Roy, D.P., Hall, D.K., Salomonson, V.V.,
708 Privette, J.L., Riggs, G., Strahler, A., Lucht, W., Myneni, R.B., Knyazikhin, Y., Running, S.W.,
709 Nemani, R.R., Wan, Z.M., Huete, A.R., van Leeuwen, W., Wolfe, R.E., Giglio, L., Muller, J.P.,
710 Lewis, P., & Barnsley, M.J. (1998). The Moderate Resolution Imaging Spectroradiometer
711 (MODIS): Land remote sensing for global change research. *Ieee Transactions on Geoscience
712 and Remote Sensing*, 36, 1228-1249

713 Kendall, M.G. (1975). *Rank Correlation Methods*. London: Griffin

714 Klein, A.G., & Stroeve, J. (2002a). Development and validation of a snow albedo algorithm for the
715 MODIS instrument. *Annals of Glaciology*, Vol 34, 2002, 34, 45-52

716 Klein, A.G., & Stroeve, J. (2002b). Development and validation of a snow albedo algorithm for the
717 MODIS instrument. *Annals of Glaciology*, 34, 45-52

718 Knap, W.H., Brock, B.W., Oerlemans, J., & Willis, I.C. (1999). Comparison of Landsat TM-derived
719 and ground-based albedos of Haut Glacier d'Arolla, Switzerland. *International Journal of
720 Remote Sensing*, 20, 3293-3310

721 Konzelmann, T., & Ohmura, A. (1995). Radiative Fluxes and Their Impact on the Energy-Balance of
722 the Greenland Ice-Sheet. *Journal of Glaciology*, 41, 490-502

723 Leiva, J.C. (1999). Recent fluctuations of the Argentinian glaciers. *Global and Planetary Change*, 22,
724 169-177

725 Li, C., Su, F., Yang, D., Tong, K., Meng, F. and Kan, B. (2017). Spatiotemporal variation of snow
726 cover over the Tibetan Plateau based on MODIS snow product, 2001–2014. *Int. J. Climatol.*
727 doi:10.1002/joc.5204

728 Li, X., Fu, W., Shen, H., Huang, C. & Zhang, L. (2017). Monitoring snow cover variability (2000–
729 2014) in the Hengduan Mountains based on cloud-removed MODIS products with an adaptive
730 spatio-temporal weighted method. *Journal of Hydrology*, 551, 314-327.

731 Liang, S.L., Stroeve, J., & Box, J.E. (2005). Mapping daily snow/ice shortwave broadband albedo from
732 Moderate Resolution Imaging Spectroradiometer (MODIS): The improved direct retrieval

733 algorithm and validation with Greenland in situ measurement. *Journal of Geophysical*
734 *Research-Atmospheres*, 110

735 Liston, G.E., & Hiemstra, C.A. (2011). The Changing Cryosphere: Pan-Arctic Snow Trends (1979–
736 2009). *Journal of Climate*, 24, 5691-5712

737 López-Moreno, J.I., Valero-Garcés, B., Mark, B., Condom, T., Revuelto, J., Azorín-Molina, C., Bazo,
738 J., Frugone, M., Vicente-Serrano, S.M., & Alejo-Cochachin, J. (2017). Hydrological and
739 depositional processes associated with recent glacier recession in Yanamarey catchment,
740 Cordillera Blanca (Peru). *Science of the Total Environment*, 579, 272-282

741 Lyapustin, A., Wang, Y., Xiong, X., Meister, G., Platnick, S., Levy, R., Franz, B., Korkin, S., Hilker,
742 T., Tucker, J., Hall, F., Sellers, P., Wu, A., & Angal, A. (2014). Scientific impact of MODIS C5
743 calibration degradation and C6+ improvements. *Atmos. Meas. Tech.*, 7, 4353-4365

744 Male, D.H., & Granger, R.J. (1981). Snow Surface-Energy Exchange. *Water Resources Research*, 17,
745 609-627

746 Malmros, J.K., Mernild, S.H., Wilson, R., Yde, J.C., & Fensholt, R. (2016). Glacier area changes in the
747 central Chilean and Argentinean Andes 1955-2013/14. *Journal of Glaciology*, 62, 391-401

748 Mann, H.B. (1945). Nonparametric Tests Against Trend. *Econometrica*, 13, 245-259

749 Marchane, A., Jarlan, L., Hanich, L., Boudhar, A., Gascoin, S., Tavernier, A., Filali, N., Le Page, M.,
750 Hagolle, O., & Berjamy, B. (2015). Assessment of daily MODIS snow cover products to
751 monitor snow cover dynamics over the Moroccan Atlas mountain range. *Remote Sensing of*
752 *Environment*, 160, 72-86

753 Masiokas, M.H., Christie, D.A., Le Quesne, C., Pitte, P., Ruiz, L., Villalba, R., Luckman, B.H.,
754 Berthier, E., Nussbaumer, S.U., González-Reyes, Á., McPhee, J., & Barcaza, G. (2016).
755 Reconstructing the annual mass balance of the Echaurren Norte glacier (Central Andes, 33.5° S)
756 using local and regional hydroclimatic data. *The Cryosphere*, 10, 927-940

757 Masiokas, M.H., Villalba, R., Luckman, B.H., Le Quesne, C., & Aravena, J.C. (2006). Snowpack
758 variations in the central Andes of Argentina and Chile, 1951-2005: Large-scale atmospheric
759 influences and implications for water resources in the region. *Journal of Climate*, 19, 6334-
760 6352

761 McClung, D.M. (2013). The effects of El Niño and La Niña on snow and avalanche patterns in British
762 Columbia, Canada, and central Chile. *Journal of Glaciology*, 59, 783-792

763 Mernild, S.H., Beckerman, A.P., Yde, J.C., Hanna, E., Malmros, J.K., Wilson, R., & Zemp, M.
 764 (2015a). Mass loss and imbalance of glaciers along the Andes Cordillera to the sub-Antarctic
 765 islands. *Global and Planetary Change*, 133, 109-119
 766 Mernild, S. H., Liston, G. E., Hiemstra, C. A., Beckerman, A. P., Yde, J. C., and McPhee, J. (2016b).
 767 The Andes Cordillera. Part IV: Spatiotemporal freshwater runoff distribution to adjacent seas
 768 (1979– 2014). *International Journal of Climatology*, 37(7), 3175–3196
 769 Mernild, S. H., Liston, G. E., Hiemstra, C. A., Malmros, J. K., Yde, J. C., and McPhee, J. (2016a). The
 770 Andes Cordillera. Part I: Snow Distribution, Properties, and Trends (1979–2014). *International*
 771 *Journal of Climatology*, 37(4), 1680–1698
 772 Mernild, S. H., Liston, G. E., Hiemstra, C. A., Yde, J. C., McPhee, J., and Malmros, J. K. (2016c). The
 773 Andes Cordillera. Part II: Rio Olivares Basin Snow Conditions (1979–2014), Central Chile.
 774 *International Journal of Climatology*, 37(4), 1699–1715.,
 775 Mernild, S.H., Liston, G.G., Kane, D.L., Knudsen, N.F., & Hasholt, B. (2008). Snow, runoff, and mass
 776 balance modeling for the entire Mittivakkat Glacier (1998-2006), Ammassalik Island, SE
 777 Greenland. *Geografisk Tidsskrift-Danish Journal of Geography*, 108, 121-136
 778 Mernild, S.H., Malmros, J.K., Yde, J.C., Wilson, R., Knudsen, N.T., Hanna, E., Fausto, R.S., & van
 779 As, D. (2015b). Albedo decline on Greenland's Mittivakkat Gletscher in a warming climate.
 780 *International Journal of Climatology*, 35, 2294-2307
 781 Meza, F.J., Wilks, D.S., Gurovich, L., & Bambach, N. (2012). Impacts of Climate Change on Irrigated
 782 Agriculture in the Maipo Basin, Chile: Reliability of Water Rights and Changes in the Demand
 783 for Irrigation. *Journal of Water Resources Planning and Management*, 138, 421-430
 784 Montecinos, A., & Aceituno, P. (2003). Seasonality of the ENSO-related rainfall variability in central
 785 Chile and associated circulation anomalies. *Journal of Climate*, 16, 281-296
 786 Moustafa, S.E., Rennermalm, A.K., Román, M.O., Wang, Z., Schaaf, C.B., Smith, L.C., Koenig, L.S.,
 787 & Erb, A. (2017). Evaluation of satellite remote sensing albedo retrievals over the ablation area
 788 of the southwestern Greenland ice sheet. *Remote Sensing of Environment*, 198, 115-125
 789 Oerlemans, J., Giesen, R.H., & Van den Broeke, M.R. (2009). Retreating alpine glaciers: increased
 790 melt rates due to accumulation of dust (Vadret da Morteratsch, Switzerland). *Journal of*
 791 *Glaciology*, 55, 729-736

792 Neckel, N., Loibl, D., & Rankl, M. (2017). Recent slowdown and thinning of debris-covered glaciers in
793 south-eastern Tibet. *Earth and Planetary Science Letters*, 464, 95-102

794 Pellicciotti, F., Burlando, P., & Van Vliet, K. (2007). Recent trends in precipitation and streamflow in
795 the Aconcagua River basin, central Chile Glacier mass balance changes and meltwater
796 discharge. In, *Foz do Iguaçu*. International Association of Hydrological Sciences: IAHS

797 Peña, H., & Nazarala, B. (1987). Snowmelt-Runoff Simulation Model of a Central Chile Andean Basin
798 with Relevant Orographic Effects. In, *International Association of Hydrological Sciences*
799 (*IAHS*). Vancouver, Canada: IAHS

800 Pfeffer, W.T., Arendt, A.A., Bliss, A., Bolch, T., Cogley, J.G., Gardner, A.S., Hagen, J.-O., Hock, R.,
801 Kaser, G., Kienholz, C., Miles, E.S., Moholdt, G., Mölg, N., Paul, F., Radi, Valentina, Rastner,
802 P., Raup, B.H., Rich, J., & Sharp, M.J. (2014). The Randolph Glacier Inventory: a globally
803 complete inventory of glaciers. *Journal of Glaciology*, 60, 537-552

804 Polk, M.H., Young, K.R., Baraer, M., Mark, B.G., McKenzie, J.M., Bury, J., & Carey, M. (2017).
805 Exploring hydrologic connections between tropical mountain wetlands and glacier recession in
806 Peru's Cordillera Blanca. *Applied Geography*, 78, 94-103

807 Prohaska, F. (1976). The climate of Argentina, Paraguay and Uruguay. In W. Schwerdfeger (Ed.),
808 *World Survey of Climatology* (pp. 13 - 112). New York: Elsevier

809 Ragettli, S., Immerzeel, W.W., & Pellicciotti, F. (2016). Contrasting climate change impact on river
810 flows from high-altitude catchments in the Himalayan and Andes Mountains. *Proceedings of*
811 *the National Academy of Sciences of the United States of America*, 113, 9222-9227

812 Riggs, G.A., Hall, D.K. & Román, M.O. (2017) Overview of NASA's MODIS and Visible Infrared
813 Imaging Radiometer Suite (VIIRS) snow-cover Earth System Data Records. *Earth Syst. Sci.*
814 *Data*, 9, 765-777.

815 Rittger, K., Painter, T.H., & Dozier, J. (2013). Assessment of methods for mapping snow cover from
816 MODIS. *Advances in Water Resources*, 51, 367-380

817 Rutllant, J., & Fuenzalida, H. (1991). Synoptic Aspects of the Central Chile Rainfall Variability
818 Associated with the Southern Oscillation. *International Journal of Climatology*, 11, 63-76

819 Saavedra, F.A., Kampf, S.K., Fassnacht, S.R., & Sibold, J.S. (2016). A snow climatology of the Andes
820 Mountains from MODIS snow cover data. *International Journal of Climatology*

821 Saavedra1, F.A., Kampf, S.k., Fassnacht, S.R., and Sibold, J.S. Changes in Andes Mountains snow
822 cover from MODIS data 2000-2014. *The Cryosphere Discuss.*, [https://doi.org/10.5194/tc-2017-](https://doi.org/10.5194/tc-2017-72)
823 72, in review, 2017.

824 Savitzky, A., & Golay, M.J.E. (1964). Smoothing and Differentiation of Data by Simplified Least
825 Squares Procedures. *Analytical Chemistry*, 36, 1627-1639

826 Sirguey, P., Still, H., Cullen, N.J., Dumont, M., Arnaud, Y., & Conway, J.P. (2016). Reconstructing the
827 mass balance of Brewster Glacier, New Zealand, using MODIS-derived glacier-wide albedo.
828 *The Cryosphere*, 10, 2465-2484

829 Sorman, A.U., Akyurek, Z., Sensoy, A., Sorman, A.A., & Tekeli, A.E. (2007). Commentary on
830 comparison of MODIS snow cover and albedo products with ground observations over the
831 mountainous terrain of Turkey. *Hydrology and Earth System Sciences*, 11, 1353-1360

832 Tedesco, M., Fettweis, X., Mote, T., Wahr, J., Alexander, P., Box, J.E., & Wouters, B. (2013).
833 Evidence and analysis of 2012 Greenland records from spaceborne observations, a regional
834 climate model and reanalysis data. *The Cryosphere*, 7, 615-630

835 Tekeli, A.E., Akyürek, Z., Arda Şorman, A., Şensoy, A., & Ünal Şorman, A. (2005). Using MODIS
836 snow cover maps in modeling snowmelt runoff process in the eastern part of Turkey. *Remote*
837 *Sensing of Environment*, 97, 216-230

838 Vuille, M., Kaser, G., & Juen, I. (2008). Glacier mass balance variability in the Cordillera Blanca, Peru
839 and its relationship with climate and the large-scale circulation. *Global and Planetary Change*,
840 62, 14-28

841 Wang, Z., Schaaf, C.B., Strahler, A.H., Chopping, M.J., Román, M.O., Shuai, Y., Woodcock, C.E.,
842 Hollinger, D.Y., & Fitzjarrald, D.R. (2014). Evaluation of MODIS albedo product (MCD43A)
843 over grassland, agriculture and forest surface types during dormant and snow-covered periods.
844 *Remote Sensing of Environment*, 140, 60-77

845 Warren, S.G., & Wiscombe, W.J. (1980). A Model for the Spectral Albedo of Snow. II: Snow
846 Containing Atmospheric Aerosols. *Journal of the Atmospheric Sciences*, 37, 2734-2745

847 Wilson, R., Mernild, S.H., Malmros, J.K., Bravo, C., & CarriÓN, D. (2016). Surface velocity
848 fluctuations for Glaciar Universidad, central Chile, between 1967 and 2015. *Journal of*
849 *Glaciology*, 62, 847-860

850 Wiscombe, W.J., & Warren, S.G. (1980). A Model for the Spectral Albedo of Snow. I: Pure Snow.
851 *Journal of the Atmospheric Sciences*, 37, 2712-2733

852 Wolter, K., & Timlin, M.S. (2011). El Niño/Southern Oscillation behaviour since 1871 as diagnosed in
853 an extended multivariate ENSO index (MEI.ext). *International Journal of Climatology*, 31,
854 1074-1087

855 Xu, W., Ma, H., Wu, D. & Yuan, W. (2017). Assessment of the Daily Cloud-Free MODIS Snow-Cover
856 Product for Monitoring the Snow-Cover Phenology over the Qinghai-Tibetan Plateau. *Remote*
857 *Sensing*, 9, 585.